FLAMELET/FLOW INTERACTION IN PREMIXED TURBULENT FLAMES: SIMULTANEOUS MEASUREMENTS OF GAS VELOCITY AND FLAMELET POSITION*

P.C. Miles
Sandia National Laboratories, Livermore, CA

F.C. Gouldin
Cornell University, Ithaca, NY

ABSTRACT

An experimental technique for obtaining simultaneous measurements of fluid velocity and flamelet position in premixed flames is described and applied in a turbulent V-flame. The flamelet position information is used to calculate conditional velocity statistics– conditional on both zone (reactants or products) as well as conditional on distance from the flamelet. The conditional zone statistics demonstrate that increases (or decreases) in turbulence across the flame are dependent on axial position and location within the flame brush. The product-zone conditional covariance, coupled with the measured conditional mean velocity profiles, indicate that turbulence generation by shear may be a significant contribution to product zone turbulence levels. Velocity statistics conditional on distance from the flamelet demonstrate a considerable interaction between the flamelet and velocity field. Mean and rms velocities vary significantly with proximity to the flamelet, such that differences in the conditional zone velocity statistics are not always representative of the differences in velocities which occur just across the flamelet surface. The change in rms velocities just across the flamelet is found to be anisotropic, with the largest increase (smallest decrease) ocurring in the axial velocity component. Rms velocities conditional on flamelet position further support the hypothesis that increased product gas velocity fluctuations may have a significant component associated with turbulence generation by mean shear.

INTRODUCTION

Recent progress towards the understanding of premixed turbulent combustion has been achieved through the development and use of conditional sampling techniques in experimental studies of the turbulent velocity field. Concurrently, wrinkled laminar flamelet models[1,2] have been developed which are formulated in terms of conditional zone statistics for gas and flow field properties. These models consider the flow field as consisting of two zones in which gas thermodynamic properties are considered to be constant; properties in one zone are characteristic of unburnt combustible mixture, while the other zone has properties characteristic of the burnt products. Separating the two zones is the laminar flamelet, which, for large scale turbulence, is a wrinkled flame with an internal structure determined by molecular diffusion processes. If the flamelet is thin compared to the region over which it moves (the turbulent flame brush), then the probability density function (pdf) of any thermodynamic property is dominated by peaks at property values characteristic of the burnt and unburnt fluid; the probability of encountering fluid with properties between the limiting values of burnt and unburnt fluid is considered negligible. Under conditions such as these, mean unconditional flow properties at any point are known in terms of the mean properties associated with each zone (conditional means) and the probability of finding the point within that zone. Similarly, the unconditional correlations associated with turbulence moment closures can all be expressed in terms of conditional zone quantities.

Other modeling approaches utilizing the ideas described above are formulated such that terms appear explicitly in the turbulence conservation equations which are associated with the velocity and pressure discontinuities across the flamelet[3]. Modeling of the entrainment terms, those terms arising from the velocity discontinuity, is achieved in part through ensemble point averages of flow quantities taken only when the flamelet is crossing the point. Experimental data from which these point averages can be determined are non-existent; obtaining such data represents an even greater experimental challenge than obtaining reliable conditional zone statistics.

Paralleling the development of statistical models are analytical studies of the interaction between a wrinkled laminar flamelet and the turbulent velocity field[4]. These studies predict the existence of a two-way interaction between the flamelet and the turbulent velocity field: turbulent velocity fluctuations cause wrinkling of the flamelet and in turn, flamelet wrinkles induce local perturbations in flow velocity and pressure which modify the turbulent velocity field. Neither the statistical theories of turbulent combustion nor theories aimed towards prediction of turbulent flame speeds explicitly model this interaction, and, indeed, experimental data related to this phenomenon are so scarce that its relative importance has not been established. The approach used in these studies also allows prediction of the relationship between the

turbulence intensities just upstream and just downstream of the high temperature reaction zone of a wrinkled flamelet[5]. Under conditions of large scale turbulence and small angles of inclination of the flamelet with respect to its mean orientation, turbulence intensities transverse to the mean flamelet surface are predicted to increase substantially, while the normal component turbulence intensity is unaltered.

From the above discussion, the utility of velocity data conditioned on distance from the flamelet is apparent. The additional information provided by the knowledge of the flamelet position allows the construction of improved conditional zone statistics which are substantially free of contamination by measurements made within the finite flamelet thickness. Furthermore, velocity data obtained immediately adjacent to the flamelet can be identified and employed to determine jumps in mean and fluctuating velocities which occur across the flamelet. Experimental determination of these jumps permits the further development of flamelet models of turbulent combustion and permits verification of the predictions of theoretical analyses. Finally, the extent to which the wrinkled flamelet and the velocity field mutually interact, both upstream and downstream of the flamelet, can be investigated.

In this paper we describe in detail an experimental technique which permits the simultaneous measurement of two components of gas velocity and flamelet position along a line nearly normal to the mean flamelet surface. Data obtained are used to compute conditional statistics (both zone statistics and statistics conditional on distance to the flamelet surface) for a lean ethylene flame which is rod-stabilized in grid generated turbulence. The experimental technique is critically evaluated and uncertainties are discussed in depth so as to establish the validity of the data obtained and the resulting statistics. Finally, statistics conditional on distance to the flamelet are presented and the implications of these statistics on the interpretation of the zone statistics and on the phenomena of flame generated turbulence are discussed.

EXPERIMENTAL APPARATUS AND METHODOLOGY

Overview of the Experiment

All measurements are obtained in a V-shaped turbulent flame stabilized on a rod at the exit of a jet of premixed reactants (Fig. 1). The experimental technique consists of the simultaneous use of two-component laser Doppler velocimetry (LDV) and laser induced Mie scattering for determination of flamelet position. The flamelet position measurement requires the reactant

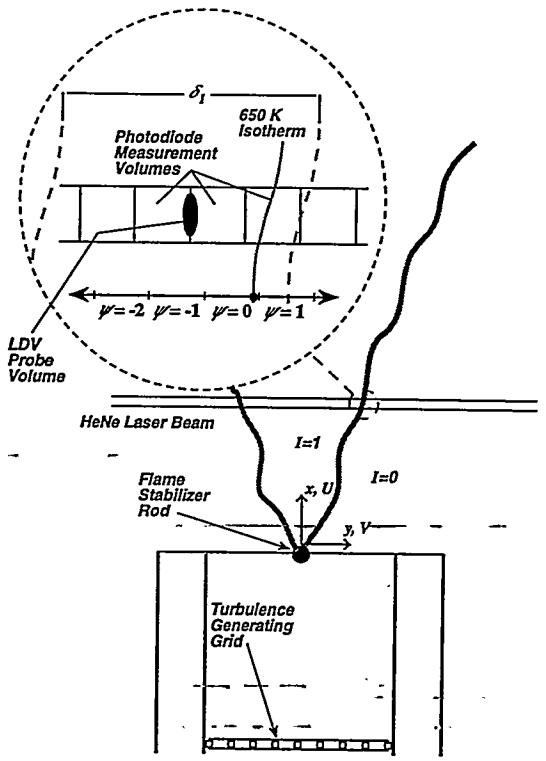

Figure 1: Schematic diagram of the burner exit, flame geometry, and coordinate systems used.

flow to be seeded with a fine oil mist, with oil particles sufficiently small that they evaporate and burn in a time which is small compared to their passage time through the flamelet. Intense Mie scattered light from a laser beam is thus observed only from those regions where the oil particles are present (unburnt reactants), and the interface between bright regions of high intensity scattered light and dark regions where little light is scattered serves to mark the intersection of the flamelet with a line defined by the laser beam. Scattered light is monitored by a photodiode array (PDA), which allows the determination of the location of the scattered light interface along the laser beam within discrete limits. Concurrently, fluid velocity is measured at various locations along the line defined by the laser beam. A small amount of refractory seed particles (ZrO_2) is also added to the flow to provide LDV scattering centers within the product fluid. The experimental layout is depicted in Fig. 2.

The Burner Facility, Turbulence Characterization, and Flame Conditions

Figure 1 details the burner exit and the coordinate system used. The origin of the coordinate system is taken to be the centerline of the exit jet at the axial location of the 1.0 mm diameter flame stabilizer rod. All measurements are made with a nominal mean axial

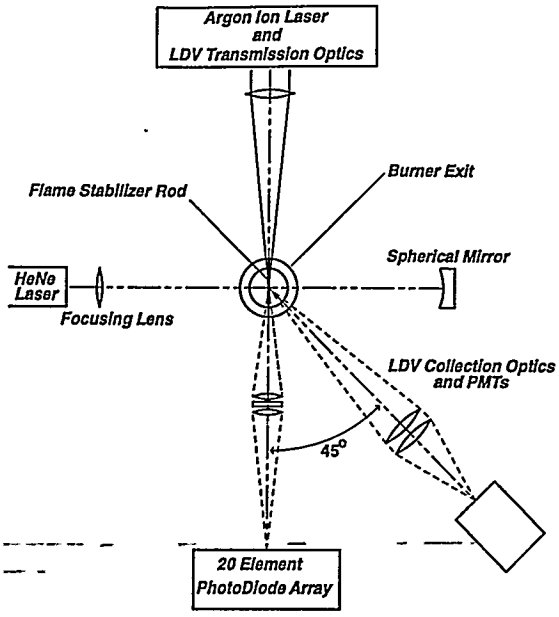

Figure 2: Layout of the experiment.

velocity of 6 m/s, measured in the cold, non-reacting jet with the flame stabilizer rod removed. Data are obtained at four different axial locations: 30, 40, 50, and 60 mm. Turbulence is generated in the exit jet of the burner by interchangeable turbulence generating grids, mounted 5.0 cm below the exit plane.

Data presented here are obtained with a bi-planar grid constructed with 1.59 mm square bars on a 6.0 mm mesh. Characteristics of the cold-flow turbulence are presented in Table 1 at the four axial locations (x) at which measurements are performed. Length scales are obtained from the measured axial velocity autocovariance function– the integral scale, ℓ, via integration to the first zero crossing and the Taylor scale, λ, via the intercept with the abscissa of a parabolic fit to the function near the origin.

Data have been obtained for a variety of flame conditions[6] (turbulence generating grids, fuels, equivalence ratios). Results reported here, however, are limited to a single $\phi = 0.69$ ethylene flame which exhibits many of the features of the other flames studied and allows close comparison to previous experimental studies[7,8]. Characteristics of this flame are provided in Table 2. Two values of the laminar flame thickness are reported. The first, δ_1, is estimated from stoichiometric flame temperature profiles[9] and the assumption that flame thickness scales inversely with the laminar flame speed. This flame thickness is based on the distance over which the central 80% of the temperature change across the flame occurs. The second definition of the laminar flame thickness, $\delta_2 = \alpha / u_L$, is chosen to be consistent with the thicknesses usually reported in the literature[10], where α is the thermal diffusivity of the reactant mixture evaluated at the mean of the cold reactant temperature and the adiabatic flame temperature. This definition is included in Table 2 to facilitate comparison between the experimental conditions employed in this study and those employed elsewhere. The large-eddy Damköhler numbers reported in Table 2 are defined by the relation $\mathrm{Da} = (\ell / u')\,(u_L / \delta_2)$. Damköhler numbers based on δ_1 are of order unity for the flames studied here. The laminar flame speed, u_L, is estimated from Cattolica, *et al.*[11]. By virtue of the characteristics summarized in Table 2, the flame studied here is thus considered to fall in the wrinkled laminar flame regime of turbulent combustion. It must be recognized, however, that the structure of the flamelets may depart from that of a laminar flame due not only to the effects of straining and flamelet curvature but also due to turbulent diffusion processes within the relatively thick flamelet preheat zone $(\delta_1 \cong \lambda)$.

Table 1

Cold Flow Turbulence Characteristics
Square Bar Grid: d=1.59 mm, M=6.0 mm

x (mm)	λ (mm)	ℓ (mm)	$\frac{1}{2}(u'+v')$(m/s)	Re_λ	Re_ℓ
30	1.8	2.8	0.33	37	56
40	1.9	2.7	0.30	35	51
50	2.0	3.2	0.27	34	55
60	2.1	3.3	0.26	35	54

The Laser Doppler Velocimeter

The apparatus used for laser Doppler velocimetry (LDV) measurements consists of an argon-ion laser (Lexel, Model 95-4) and commercial optics with a Bragg cell frequency shifter and 2.27X beam expansion (Thermosystems, Inc., 9100 series) for focusing the

Table 2

Flame Characteristics
Ethylene, ϕ=0.69

u_L	0.32	(m/s)
δ_1	2.2	(mm)
δ_2	0.06	(mm)
u'/u_L	0.9	
Da	53	
Re	55	
ρ_r/ρ_p	6.24	

incident beams and collecting the scattered light. A 5.0 MHz frequency shift is used in one of the lateral component beams to remove directional ambiguity. Scattered light is collected by a 250 mm focal length lens along a horizontal axis 45 degrees from the perpendicular to the incident radiation. The LDV measurement volume defined by the laser wavelength and optics has a minor axis diameter of 0.06 mm, and a major axis diameter of about 0.44 mm, aligned parallel to the flame stabilizer rod. Figure 2 represents schematically the location of the LDV components as well as the components of the flamelet position measurement system.

The entire LDV apparatus, including the collection optics, is situated on an optical breadboard with translation capability in the lateral y-coordinate direction. This configuration allows for a lateral scan of the flow field while leaving the burner stationary and without disturbing the optical alignment. The breadboard is positioned with a stepper motor driven lead screw having a resolution of 2.5 μm and an accuracy of better than 12.5 μm/m.

LDV signal processing is accomplished with counter-type signal processors (Thermosystems, Inc., Model 1990B and Model 1990C), set to time 16 cycles with an internal validation setting of 1%. These settings represent the most stringent data timing and validation conditions permitted by the optical setup and signal processors. The best amplification level of the LDV signals prior to timing is determined by varying the gain of the signal processors and evaluating the effect on the measured rms velocities in both unburnt reactants and the burnt products. Due to the care taken in the introduction of LDV seed particles (see the discussion below), it is possible to vary the gain by more than an order of magnitude without affecting the turbulence statistics. The same gain could therefore be used at all locations within the flame while obtaining noise-free data at adequate data rates. At the selected operating point, data rates within the reactants exceeded 50 kHz and within the products data rates were approximately 2 kHz. Note that this large disparity in data rates is due to the combined effects of volume expansion and the vaporization of oil seed particles across the flame.

The Mie Scattering System

A schematic view of the experimental apparatus used for the flamelet position measurements is also presented in Fig. 2. The laser beam used to define the line along which the flamelet position is measured is provided by a 10 mW He-Ne laser operating at 632.8 nm (Melles Griot model 05-LHP-991). The laser beam is focused to a waist of approximately 0.37 mm by an f=500 mm plano-convex lens. Laser power is effectively increased by passing the beam over the burner a second time using a spherical concave mirror with a radius of curvature of 600 mm. The effect of the spatial fluctuations in beam position incurred using this multi-pass technique is estimated to be an increase in the effective beam waist to no more than 0.52 mm.

Scattered light from the beam is collected and collimated by an *f*/3.6 achromatic lens positioned such that the lens centerline is perpendicular to the laser beam, in a plane inclined 15° below the horizontal. The collimated light is filtered by a 10 nm FWHM bandpass filter centered at 632.8 nm and then focused onto the photodetector using a second *f*/7.7 achromat. The collection system, composed of the two lenses and the filter, is characterized by a measured magnification of 2.14 and a resolution on axis and 5.0 mm off axis of 6 and 42 μm, respectively.

The photodetector employed is a 20 element linear photodiode array (EG&G Photon Devices PDA 20-3), characterized geometrically by an element center-to-center spacing of 1.0 mm and an element active area size of 4.0 mm by 0.94 mm. Note that the spacing between the active areas of the elements (60 μm) is greater than the resolution of the optical system, thus minimizing the possibility of inter-element cross-talk due to optical system resolution. The array surface optical response uniformity and element cross-talk are both specified to be better than 1% for radiation at 632.8 nm. The spatial resolution of the flamelet position measurement is determined by the portion of the laser beam imaged on each element of the PDA, and is characterized by a cylindrical volume with a diameter given by the diameter of the laser beam waist and a length equal to the length of the beam imaged on an element. With the optical system employed, this volume is approximately 0.52 mm in diameter and 0.47 mm long.

Each array element outputs a continuous signal current, which is amplified by a transimpedance amplifier with a -3 dB bandwidth of 20 kHz ($\tau \approx 8\ \mu s$). Additional stages of amplification are of sufficient bandwidth that the overall frequency response is determined by this first stage amplifier. Provision is made for gain and offset trimming in each channel. Offset trimming is provided not only to compensate for thermal drift, but also in anticipation of a dc component to the scattered light from ZrO_2 particles in the burnt products. Thermal drift is negligible after a short warm-up period, and it is found that scattered light from the products has a negligible dc component.

The amplified signal from each element is digitized by a comparator with a threshold set at 10% of the full scale signal obtained when the portion of the laser beam

imaged on the element was fully within the reactants. Selection of this threshold is discussed below. A small amount of hysteresis (0.2% of the full scale signal) is provided to help prevent oscillation caused by electronic or marker shot noise during slow signal transitions. The processed signals from each element in the array constitute a 20-bit digital 'word', where the state of each bit indicates whether the signal from the corresponding element is above or below a level of 10% of the full scale signal. The flamelet position along the beam is determined by searching the digital word for the transition between a series of bits of value 0 and a succeeding series of bits of value 1.

Particle Seeding

Successful, simultaneous implementation of the LDV and flamelet position measurement techniques impose the following requirements on the oil and refractory particle seeding systems:

(1) Both oil and refractory particles must be small enough to follow the turbulent velocity fluctuations with a high degree of fidelity. Similarly, refractory particles must be small enough to follow the flow acceleration across the flamelet. These requirements can be met by particles with diameters of less than 6.7 μm and 2.0 μm for oil and ZrO_2 particles, respectively[6].

(2) Oil particles must be sufficiently small that they evaporate in a time which is small as compared to the time which would be required for their passage through the flamelet. This imposes an upper limit of approximately 10 μm on the particle diameter[12].

(3) 'Spikes' in the signals from the PDA elements due to scattered light from refractory particles within the products must be small compared to the 10% digitizing threshold of the flamelet position measurement system, thereby avoiding multiple transitions in the flamelet position word.

(4) The energy consumed or released upon evaporation or combustion of the oil particles must be small as compared to the energy released by the combustible mixture. This last criterion is imposed to ensure that the presence of the oil seed does not significantly alter the structure of the flame studied.

Oil seed particles are generated with a blast atomizer, which typically produces a range of particle sizes with a log-normal size distribution. Removal of the large particles in the distribution is achieved through use of a Stairmand[13] high-efficiency, long-cone, cyclone separator. The Stairmand design has been experimentally evaluated under both design and off-design flow conditions[14], which enables estimates of its performance at various flow rates to be pursued with confidence. For the operating conditions employed, a fractional collection efficiency of 50% is expected for particles with diameters of approximately 1.7 µm. Efficiencies greater than 90% are expected for oil particles larger than 3.0 µm. This clearly satisfies the restrictions placed on the particle sizes by the criteria listed above. The cyclone discharges directly into the base of the burner, minimizing the possibility of particle agglomeration.

Based on the rate of depletion of the silicone oil reservoir (and subsequent recovery from the cyclone), an oil mass fraction of approximately $4 \cdot 10^{-4}$ grams of oil per gram of combustible mixture is expected at the burner exit. With a heating value of about 6.2 cal/gm for the silicone oil used, it can be easily verified that the heat release associated with combustion of the oil is negligible in comparison to the combustible mixture.

A brief digression on the unexpected benefits provided by the cyclone separator on the flamelet position measurement signal-to-noise ratio and LDV data rates is in order. Because the signals from the PDA are digitized based on being above or below a given threshold, a large signal-to-noise ratio is not required. The cyclone separator was needed to eliminate large oil particles which persist through the flame and could thereby contaminate the velocity data, and it was expected that the signal-to-noise ratio from the photodiodes would suffer as particles were removed from the flow. Although the photodiode signal levels dropped significantly when the cyclone was employed, the signal-to-noise ratio remained approximately constant. This indicates that the noise had a significant component due to the presence of large particles as well as a component associated with variation of the number of particles in the measurement volume (marker shot-noise). In addition, the maximum LDV data rates obtainable without significant increases in measured rms velocities increased by a factor of three.

Refractory particles were introduced in the flow with a nebulizer based seed particle generator[15]. Zirconia powder (TAM ceramics, Zirox® TR) was maintained in a 4.0% (by volume) water suspension and atomized by two medical nebulizers (RETEC X70) operated in parallel at a supply pressure of 425 kPa. The atomized solution is mixed with dilution air, dried, and passed through a cyclone separator. Under the operating conditions employed, the droplet size distribution produced by the nebulizers is characterized by a mass median diameter of approximately 3.2 μm[16], and a geometric standard deviation of 2.2. The size distribution of the zirconia powder, supplied by the manufacturer, indicates a mass median diameter of approximately 0.85 μm– well below that of the droplets produced by the nebulizer. The estimated mass mean diameter of the residual particle obtained after drying of

the droplets is 1.1 μm; the count mean residual particle diameter is estimated as 0.2 μm.

The above estimates demonstrate that the vast majority of refractory seed particles are sufficiently small to follow both the turbulent velocity fluctuations and the flow acceleration across the flamelet. Due to the original log-normal droplet size distribution produced by the nebulizers, however, occasional large residual particles are expected with diameters which may be on the order of tens of microns. The existence of these large particles was observed experimentally as large 'spikes' in the signal obtained from PDA elements on which a portion of the laser beam well within the product gases was imaged. The amplitude of these spikes was sufficient to cause the signals from these array elements to erroneously cross the digitizing threshold. As with the oil seed generating system, these large particles were removed utilizing a second cyclone separator, which discharged directly into the base of the burner. Under the selected operating conditions, particles of diameter 2.4 μm and 5.7 μm are expected to experience fractional collection efficiencies of 50% and 90%, respectively.

Data Acquisition

At each lateral location 20,000 simultaneous velocity and flamelet position data are recorded; each datum is a triplet consisting of two components of gas velocity and the 20-bit flamelet position word. The flamelet position word is latched on the occurrence of a validated velocity measurement from the lateral (y) coordinate velocity channel. If a validated axial (x) coordinate velocity measurement occurs (occurred) within a 10 μs coincidence window of the lateral velocity measurement the datum is transferred to the computer.

Due to the large disparity in the seed particle number density (and thence LDV data rates) between unburnt reactants and burnt products, it is difficult to ensure that a sufficient number of velocity data are collected in the burnt gases at each measurement location. To overcome this difficulty, a histogram of flamelet position at each axial location is first determined from 20,000 clock-driven, un-biased samples of the PDA. From this histogram, the probability of finding the LDV probe volume instantaneously in zones of burnt products, unburnt reactants, or within the finite thermal thickness of the flame is determined. This information is passed to the data acquisition driver which collects the simultaneous velocity and flamelet position triplets and subsequently stores them in proportion to the measured probabilities. When the appropriate number of data corresponding to the unburnt reactant zone, say, have been acquired and stored, any additional "reactant" data are discarded and data acquisition continues until sufficient data in the other zones have been obtained. We estimate that at some locations within the flame brush as many as 10^7 data triplets are collected before a sufficient number of burnt gas zone measurements are obtained. Additionally, the data acquisition driver incorporates a software delay to ensure that the data collected are statistically independent and checks the flamelet position word for multiple transitions. The significance of these multiple transitions is discussed below.

DATA INTERPRETATION

Interpretation of the Scattered Light Signal

Interpretation of the measured scattered light signal in terms of the location of the flamelet along the laser beam must be handled with care due to the finite thermal thickness of the flame. Fundamental to this interpretation is the assumption that the scattered light interface is thin in comparison with both the characteristic dimensions of the flamelet position measurement volume (≈0.5 mm) and the thermal thickness δ_l of the flamelet. Because the time required for evaporation or burning of the oil particles is approximately 10^{-5} s,[17] while the passage time of the particles through the flamelet is on the order of 10^{-3} s, this assumption is easily satisfied. The location of the interface within the finite thickness flamelet is estimated by noting that thermogravimetric analysis of the silicone oil employed shows that negligible weight loss occurs over long periods of time at temperatures of up to 425 K, while the open cup flash point and autoignition temperature are specified to be 591 K and 708 K , respectively. Evidently vaporization begins at a gas temperature greater than 425 K, and is well under way at a temperature of 600 K. Finite-difference simulations of a silicone oil droplet passing through a stoichiometric methane-air flame further demonstrate that, even if no vaporization occurs below 600K, all particles with diameter less than 5 μm have evaporated before a local gas temperature of 800 K is reached[12]. Based on these observations, the interface is considered to represent an isotherm within the flamelet of approximately 650 K. The interpretation of the scattered light signal is not sensitive to the accuracy of this estimate due to the large temperature gradients in the flamelet; an error of ±200 K would not substantially change the conclusions reached.

The flame coordinate ψ

Due to the digital nature of the flamelet position measurement, the location of the intersection of the flamelet with the laser beam is only known to lie in

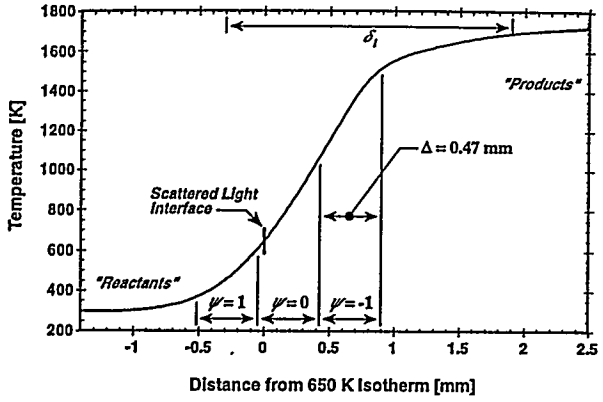

Figure 3: Estimated temperature profile of a ϕ=0.69 C_2H_4 flame. The values of ψ associated with velocity measurements made in regions with large temperature and density gradients are shown, along with the location of the scattered light interface. The resolution of the flamelet position measurement, Δ, determines the width of the region associated with each value of ψ. Also shown is the flamelet thermal thickness, δ_l, defining the region over which the central 80% of the temperature rise occurs.

regions defined by discrete lateral coordinates. The width of these regions Δ is equal to the measurement spatial resolution, which is determined by the element to element spacing of the PDA and the optical system magnification– Δ=0.47 mm. To identify the region in which the intersection is found the lateral coordinate ψ is introduced. The ψ-coordinate, having only integer values, is proportional to the lateral coordinate y of the LDV measurement volume minus the instantaneous lateral coordinate of the flamelet. With this interpretation, the ψ-coordinate is in a moving coordinate system attached to the flamelet. If ψ is greater than zero the velocity measurement volume is on the reactant side of the origin of the ψ–coordinate system, while for ψ less than zero the velocity measurement volume is on the product side. Formally, the value of theψ-coordinate is defined in terms of a scattered light interface which is nearly normal to the beam–

$$\psi = \text{Round}\left(\frac{y_{LDV\ Volume} - y_{Interface}}{\Delta} - 0.1 + 0.5\right); \qquad (1)$$

the offset 0.1 arises from the 10% digitizing threshold of the PDA electronics and the fact that the LDV probe volume is always positioned on the boundaries of the regions of the beam imaged onto each PDA element. This is illustrated in the inset of Fig. 1, where the ψ-coordinate system, its relationship to the location of the LDV measurement volume, and the discrete PDA measurement volumes are depicted.

Finite flamelet thermal thickness

As can be inferred from the inset of Fig. 1, velocity measurements obtained when ψ is near zero are actually realized within the finite flamelet thermal thickness– where fluid properties (and velocities) are characteristic of neither the unburnt reactants nor the burnt products. This observation is further illustrated in Fig. 3, where the location of the scattered light interface and the various regions associated with each value of ψ are shown within the temperature profile of a ϕ=0.69, C_2H_4 flame. The temperature profile is obtained from published stoichiometric profiles[9], with temperature scaling as the adiabatic flame temperature, thickness scaling as $1/u_L$, and an assumption of profile self-similarity. The flamelet thermal thickness δ_l, as defined earlier, is also shown. It is clear from Fig. 3 that at least three of the values of ψ correspond to regions in which velocity measurements are made in fluid where the thermodynamic state is representative of neither reactants nor products, but an intermediate state. These regions will be referred to hereafter as "flame regions."

ERRORS AND UNCERTAINTIES

The dominant sources of error, uncertainty, or bias in the data reported here are associated with finite bandwidth of the PDA electronics, the combined effects of a low PDA digitizing threshold with the presence of large refractory seed particles, and the effects of extreme flamelet orientations and/or curvature. Other possible error sources are found to be negligible[6].

Limited PDA electronic bandwidth can cause an error in the measured value of ψ when the rate of change of flamelet position along the beam is large (>10 ms^{-1}). This effect is only important when the portion of the beam imaged on the PDA is initially within a region of high scattered light (reactants) and makes a rapid transition to a region of low scattered light (products), due to the asymmetry of the digitizing threshold. The sense of this error is such that a velocity measurement realized at a $\psi = n$ is erroneously assigned to a $\psi = n+1$; that is, data obtained just on the product side of the flamelet (ψ=-2) may be assigned to a value of ψ within the flamelet (ψ=-1), or data obtained within the flamelet (ψ=1) may be identified with a ψ-coordinate just on the reactant side of the flamelet (ψ=2). Using measured rates of change of flamelet position[18], the probability of such an error is conservatively estimated to be approximately 7%. Note that this error is only important if large gradients in velocity with respect to theψ-coordinate exist. Where these gradients are largest, at and within the flamelet, the effects of this error are mitigated considerably by the counteracting effects of seed particle density bias.

As noted earlier, large refractory particles in the burnt gases may scatter sufficient light to cross the digitizing threshold of the PDA electronics. Although checking the flamelet position word for multiple transitions eliminates most of these events, it is not possible to identify this error when it occurs adjacent to the true transition in the PDA signals. Estimates of the probability of this error range from 0.25% to 2%, depending on the time elapsed since the last maintenance of the refractory particle seeding system. Like the error associated with PDA electronic bandwidth, the sense of this error is to erroneously assign a ψ value of n+1 to a velocity measurement realized at $\psi = n$.

Flamelet orientations which are not perpendicular to the laser beam have the effect of reducing the distance from the LDV measurement volume to the interface which is associated with each value of ψ. This effect is due to the fact that the flamelet thermal thickness projected onto the beam is larger than δ_1 by a factor inversely proportional to the direction cosine between the flamelet surface normal and the beam. The regions shown in the temperature profile of Fig. 3 therefore appear narrower and are translated somewhat with respect to a fixed isotherm within the flamelet. Velocity measurements obtained at relatively large $|\psi|$ may therefore have been realized within the thermal thickness of the flame. This difficulty is minimized by selecting a low digitizing threshold for the PDA signals, and is the major factor behind the selection of the 10% digitizing threshold used here. Selection of a low threshold can be shown to ensure that the actual distance from the flamelet surface to the LDV probe volume more closely approximates the distance that one would infer based on the ψ-coordinate[6].

Finally, estimates of the scales of flamelet curvature, based on the measured turbulence scales, indicate that the majority of flamelet wrinkles are expected to be larger than the characteristic dimension of the flamelet position measurement volumes associated with each PDA element. Under these circumstances, the major effect of flamelet curvature is expected to be a change in the local orientation with which the flamelet crosses the laser beam, the effect of which has been discussed above. Additionally, however, large scale curvature presents the additional possibility of multiple flamelet crossings of the He-Ne beam. These multiple crossings are difficult to distinguish unambiguously from errors which can occur due to a large refractory particle in the burnt gases; velocity measurements obtained when multiple crossings occur are discarded. This presents the possibility of introducing a bias into the measured velocity statistics. The frequency of multiple crossing events, independent of errors associated with large refractory particles, can be readily determined by sampling the PDA with no refractory particles present in the flow. For the flame condition reported here, this frequency varied from less than 2% at x=30 mm to slightly greater than 9% at x=60 mm.

DATA REDUCTION

For each LDV probe volume position, un-biased estimates of the probability of encountering the probe volume at each ψ-coordinate $P(\psi)$ are determined from 20,000 clock-driven, slowly-sampled flamelet position data. Additionally, the flamelet position data are used to determine the mean value of an indicator function, $\langle I \rangle$, at multiple locations along the laser beam. The indicator function is defined by $I(\mathrm{x})=0$ if the location x is in a region of intense scattered light characteristic of reactant fluid, $I(\mathrm{x})=1$ otherwise (see Fig. 1). For infinitely thin flames, $I(\mathrm{x}) = c(\mathrm{x})$, where $c(\mathrm{x})$ denotes the reaction progress variable commonly employed in flamelet models of turbulent combustion. The mean indicator function will be identified as the mean reaction progress variable $\langle c(\mathrm{x}) \rangle$ throughout the remainder of this work.

Statistics of velocity conditioned on ψ are computed by segregating the velocity data according to the ψ-coordinate in which they were obtained and computing the statistics of the resulting subsets of data. Although the LDV data are relatively free of noise, the velocity probability density functions (pdfs), particularly within the reactants, show occasional outliers. To better approximate the higher moments of these pdfs, these outliers are removed through application of Chauvenet's criterion[19]. No conditional statistics are computed for ψ-coordinates at which less than 200 velocity measurements were obtained. The conditional velocity pdfs are smoothed with an 8 point sliding average filter prior to presentation. This filtering preserves the relevant features of the pdfs, while reducing the statistical scatter, and is performed solely to facilitate the presentation of the results. Velocity statistics conditional on ψ are identified by the subscript n, where n is the integral value of ψ. For example, $P_1(V)$ is the conditional pdf of the lateral (V) component of velocity, conditional upon ψ having the value 1. Similarly, $\langle v_1'^2 \rangle$ is the variance of $P_1(V)$.

Conditional zone statistics are obtained from the statistics conditional on ψ by weighting each statistic by the probability of finding the LDV probe volume at the associated ψ-coordinate $P(\psi)$ and summing over the relevant values of ψ:

$$\langle V_r \rangle = \frac{\sum_{j>1} P(j) \langle V_j \rangle}{\sum_{j>1} P(j)} \quad \text{(Reactant zone)}$$

and

$$\langle V_p \rangle = \frac{\sum_{j<-1} P(j)\langle V_j \rangle}{\sum_{j<-1} P(j)} \quad \text{(product zone).} \qquad (2)$$

The "flame regions" ($\psi = -1$, 0, and 1) are not included in the computation of the conditional zone statistics.

Unconditional statistics are also computed from the statistics conditional on ψ, in a manner analogous to that expressed by Eqs. (2). All of the data obtained are included in the calculation; that is, the summation is carried out over all j. The unconditional quantities are distinguished by the subscript "UNC", e.g., $\langle U_{UNC} \rangle$ is the unconditional mean axial velocity. These unconditional statistics are expected to be free of both density bias and bias due to the large disparity in LDV data rates between reactants and products, except to the extent that contributions from the flame regions are influenced by these bias effects.

RESULTS AND DISCUSSION

Conditional Velocity Pdfs

The effectiveness of the measurement technique and the quality of the data obtained is best demonstrated through examination of the conditional velocity pdfs. These pdfs also experimentally verify various aspects of the interpretation of the flamelet position signal described earlier.

In Figs. 4 and 5 velocity pdfs conditional on ψ are presented. These pdfs are obtained from data collected at x=50.0 mm, and at a location within the flame brush where the mean reaction progress variable $\langle c \rangle$=0.6. To reduce graphical clutter, only the pdfs associated with values of ψ near zero, as well as a few pdfs at values of ψ representative of locations well within the reactants or the products, are presented.

The pdfs of the lateral component of velocity, in which the largest jump in conditional mean velocity across the flamelet occurs, show a distinct separation between conditional pdfs associated with the products (ψ negative) and those associated with reactants (ψ positive). This separation clearly demonstrates the success of the technique in conditioning the velocity data. Pdfs associated with the flame regions, $\psi = 1$, 0, and -1, behave as expected given the interpretation of the flamelet position signal discussed earlier. The pdf conditional on $\psi = 0$ is characterized by velocities spanning those characteristic of reactants and those of products, conforming with the expected flow acceleration associated with gas temperature or density changes across the flamelet. Similarly, pdfs conditional on $\psi = 1$ and $\psi = -1$ exhibit shifts toward velocities characteristic of products or reactants, respectively.

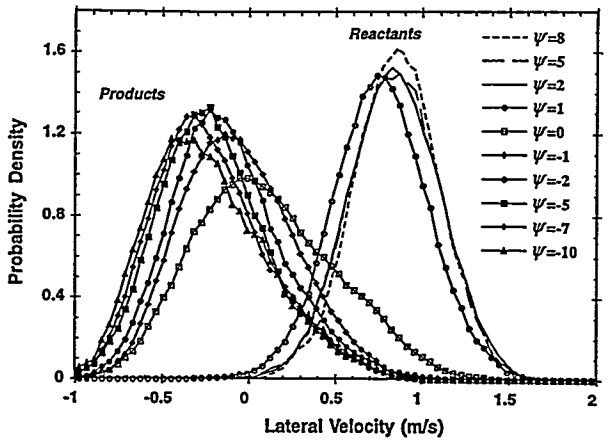

Figure 4: Probability density functions of the lateral component of velocity at x=50.0 mm and at a lateral location where $\langle c \rangle$=0.60, conditional on distance from the flamelet (ψ). The curves with filled symbols correspond to velocity measurements made in the product gases ($\psi < -1$), the curves with open symbols correspond to measurements made within the thermal thickness of the flamelet($-1 \leq \psi \leq 1$), and the curves without symbols correspond to measurements obtained within the reactants ($\psi > 1$).

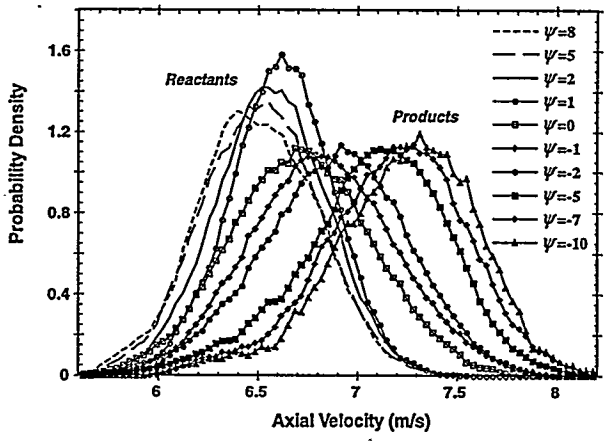

Figure 5: Conditional probability density functions of the axial component of velocity obtained under the same conditions as the lateral component pdfs shown in Fig. 4.

The breadth of the lateral component pdfs obtained within product gases is approximately equal to the breadth of the pdfs obtained in the reactant gases. This indicates little change in the turbulence levels across the flamelet. In addition, note that the product gas pdfs exhibit a positive skewness. Recalling that, for large angles between the flamelet surface normal and the HeNe laser beam, data obtained within the flamelet thermal thickness may be assigned to a large $|\psi|$, this skewness may be an artifact of extreme flamelet orientations. For flames in which multiple crossing

events (and therefore extreme flamelet orientations) are less frequent, the skewness of the conditional pdfs is observed to decrease considerably. For this reason, we believe that this skewness is, at least in part, an artifact of the measurement technique. The variance of these pdfs is thus an overestimate of the true variance.

The conditional pdfs of the axial component of velocity shown in Fig. 5 show less separation between pdfs associated with negative ψ values and those associated with positive ψ values than the lateral component pdfs, due to the smaller acceleration across the flamelet in this coordinate direction. Similar to the lateral velocity component pdfs, the axial component pdfs also exhibit a skewness (although negative in this case), which may be attributed to the effects of extreme flamelet orientations. Apart from this observed skewness, the breadth of the pdfs at negative values of ψ can be clearly seen to be larger than the pdfs associated with positive values of ψ, indicating an unambiguous increase in axial component turbulence levels.

Another notable feature of the axial component pdfs is the continued positive acceleration in the mean axial velocity as ψ becomes increasingly negative. This is evidenced by the systematic "marching" of the conditional pdfs toward higher mean axial velocities. No behavior of comparable character is observed in the lateral component pdfs, where the majority of the acceleration in the mean lateral velocity occurs over the flame regions, ψ = -1, 0, 1. It is clear that this systematic variation of the conditional mean will result in a large conditional product-zone axial velocity variance.

Unconditional and conditional zone statistics

In this section we present unconditional and conditional zone (product or reactant) profiles of mean and rms velocities, as well as the velocity field covariance, for four different axial locations. The mean profiles illustrate the global flow geometry, and allow the difference in conditional zone mean velocities and the evolution of this difference across the flame brush to be examined. Similarly, profiles of the rms velocities permit the differences in turbulence levels between reactant and product zones (and the evolution of these differences) to be evaluated. Finally, the velocity field covariance profiles, coupled with the mean velocity profiles, provide insight into the importance of turbulence generation by shear in the product and reactant zones.

Conditional zone statistics have been reported previously by Cheng and co-workers[7,8] in similar flames. Our results are generally consistent with their work, and most of the differences which do exist can be attributed to small differences in experimental conditions[6]. Significant differences between the results are discussed explicitly below.

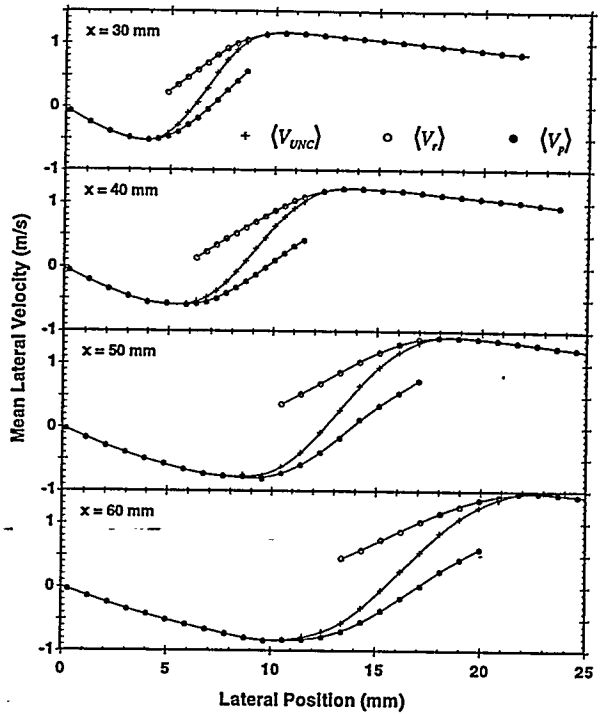

Figure 6: Mean lateral velocity– unconditional and zone conditional (products or reactants) lateral coordinate profiles

Mean profiles of the lateral velocity component are presented in Fig. 6. The region of positive mean velocity at the larger lateral (y) coordinates corresponds to pure reactants, where the mean flow is deflected outward by the volume expansion occurring within the turbulent flame brush. Within the turbulent flame brush, data exist for both conditional zones, and an inward acceleration in the mean flow is observed. Note that for infinitely thin flames, the unconditional mean velocity can be expressed as a weighted sum of the conditional zone means,

$$\langle V_{UNC} \rangle = (1-\langle c \rangle)\langle V_r \rangle + \langle c \rangle \langle V_p \rangle \,, \qquad (3)$$

and therefore can be expected to vary smoothly between the conditional zone mean velocities. In contrast to previous work, we find that the difference between the conditional reactant and product zone mean velocities, $\langle V_r \rangle - \langle V_p \rangle$, is not constant but can increase considerably as the product side of the flame brush is approached. The magnitude of this increase is approximately 70% at the higher axial locations. This observation is of theoretical significance, as the jumps in conditional zone turbulence quantities are often modeled in terms of the jumps in the mean conditional zone velocities[1]. Finally, within the product gases, the

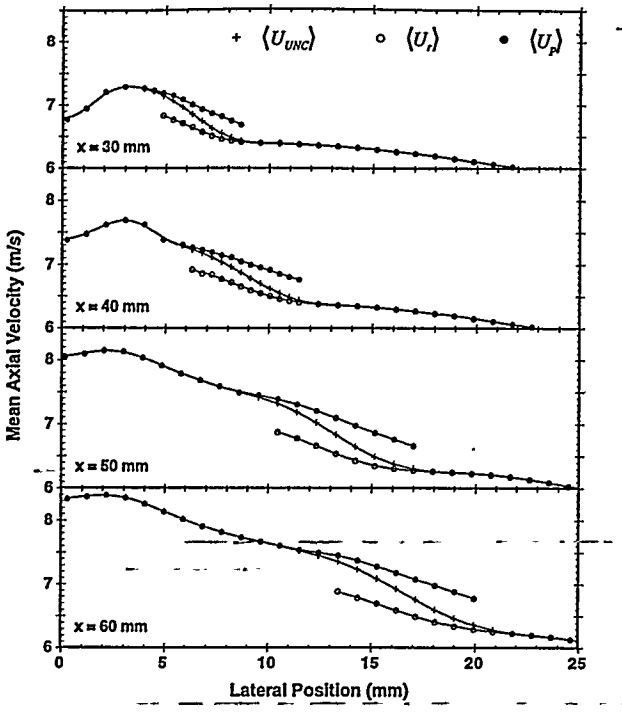

Figure 7: Mean axial velocity– unconditional and zone conditional (products or reactants) lateral coordinate profiles.

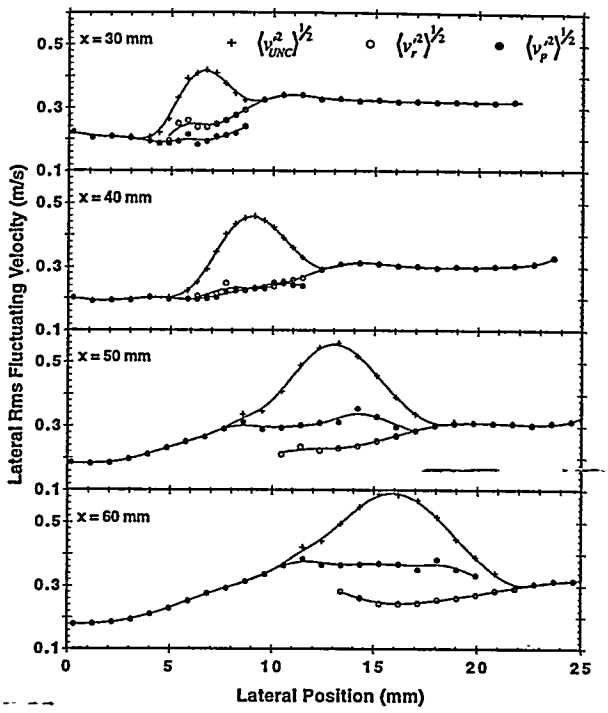

Figure 8: Lateral rms turbulence levels– unconditional and zone conditional lateral (y) coordinate profiles.

mean flow is deflected upward to satisfy symmetry conditions at the burner centerline.

Profiles of the mean axial component of velocity are shown in Fig. 7. As with the lateral component profiles, an acceleration across the flame brush is observed, resulting in a higher axial velocity within the product gases. Note that the remnants of the wake of the flame stabilizer rod are clearly visible near y=0, even at the highest axial location. Self-consistency between the measured lateral and axial component mean data can be examined by computing conditional zone mass fluxes and estimating mean reaction rates from conditional conservation equations. The resulting reaction rates are quite reasonable[20], thus demonstrating the consistency of the data obtained.

Rms lateral turbulence level profiles are presented in Fig. 8. The unconditional profiles show a distinct peak within the flame brush, which is due to measuring intermittently in regions of differing mean velocities. Like the mean velocities, the unconditional turbulence levels can be expressed in terms of the conditional zone statistics:

$$\langle v'^2_{UNC}\rangle = (1-\langle c\rangle)\langle v'^2_r\rangle + \langle c\rangle\langle v'^2_p\rangle + \langle c\rangle(1-\langle c\rangle)\left(\langle V_p\rangle - \langle V_r\rangle\right)^2. \quad (4)$$

The term multiplying the difference in conditional zone mean velocities is the contribution due to intermittency, and can be a significant, if not the dominant, source of apparent turbulence in the unconditional statistics. Turbulence levels within the reactants are approximately constant, and tend to decrease as the flame brush is traversed. Product gas turbulence levels are approximately constant within the flame brush, and tend to either remain constant or decrease as the burner centerline is approached.

Note that a distinct increase in conditional zone turbulence levels going from the reactant to the product zone is observed at the higher axial locations. Conversely, at the lowest axial location a clear decrease is observed. This difference implies that the flame may not be a source of turbulence, *per se*, but that turbulence enhancement across flames is affected by local flow conditions as well as the local statistical geometry of the flame.

The profiles of the axial component unconditional and conditional zone rms turbulence levels are presented in Fig. 9. Profiles of $\langle u'^2_r\rangle^{1/2}$ are approximately constant within the reactants and decrease as the flame brush is traversed towards the products. Unconditional profiles of rms velocities are similar to the lateral component profiles, again showing a peak within the flame brush associated with intermittency. Profiles of conditional rms turbulence levels within the products, $\langle u'^2_p\rangle^{1/2}$, exhibit a bell-like shape within the flame brush, indicating that the generation of axial component

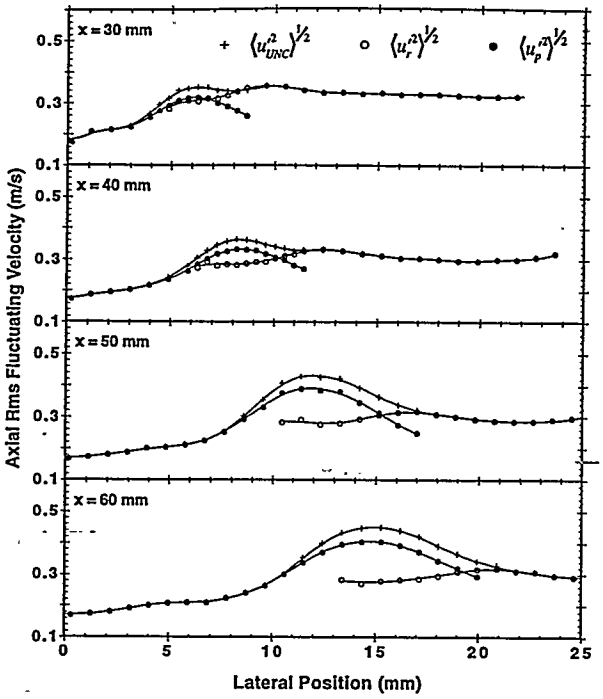

Figure 9: Axial rms turbulence levels– unconditional and zone conditional lateral (y) coordinate profiles.

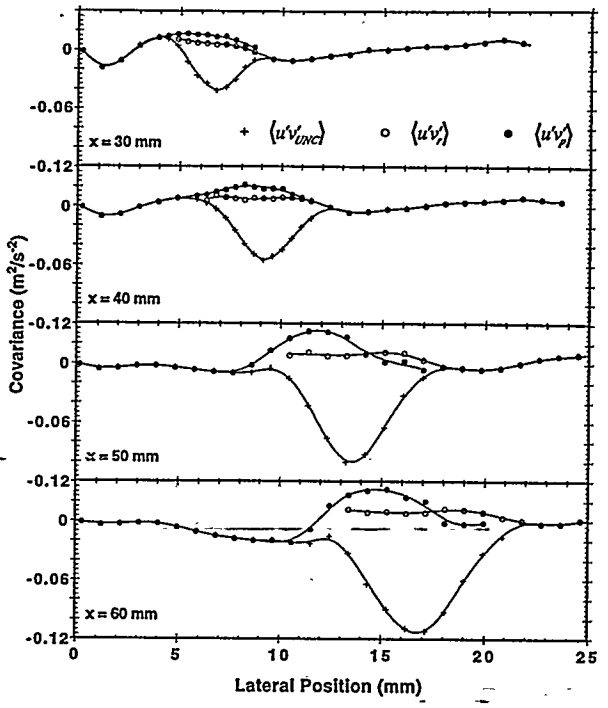

Figure 10: Velocity field covariance–unconditional and zone conditional lateral (y) coordinate profiles.

turbulence is not constant across the flame brush. Product gas turbulence levels exceed the reactant levels on the product side and in the center of the flame brush at all axial locations, while on the reactant side of the flame brush $\langle u_p'^2\rangle^{1/2}$ falls below $\langle u_r'^2\rangle^{1/2}$.

The unconditional covariance shown in Fig. 10 exhibits a large negative peak associated with intermittency, consistent with the relation

$$\langle u'v'_{UNC}\rangle = (1-\langle c\rangle)\langle u'v'_r\rangle + \langle c\rangle\langle u'v'_p\rangle + (1-\langle c\rangle)\langle c\rangle\left(\langle U_p\rangle - \langle U_r\rangle\right)\left(\langle V_p\rangle - \langle V_r\rangle\right), \quad (5)$$

while the reactant zone covariance maintains moderately constant, low levels at all locations. The product zone covariance, however, shows a positive peak within the flame brush, in contrast to previously obtained results[7,8]. The magnitude of this peak is significant: when normalized by the corresponding conditional rms velocities, the peak covariance coefficient obtained is approximately 0.3 for the profiles shown in Fig. 10. Note that the positive values of the covariance coefficient could not be caused by the effects of extreme flamelet orientations, which would tend to make the measured covariance more negative. The reported values of $\langle u'v'_p\rangle$ should therefore be considered an underestimate of the true conditional covariance within the product zone.

A positive covariance, coupled with the negative signs of both $\partial\langle V_p\rangle/\partial x$ and $\partial\langle U_p\rangle/\partial y$, indicates that shear stresses are a source of turbulent kinetic energy within the product zone. It is, perhaps, not coincidental that the location of maximum product zone covariance in Fig. 10 is well correlated with the maximum product zone turbulence levels shown in Fig. 9. This is an important observation, in that both theoreticians and experimentalists have assumed that production of turbulence by shear in these unconfined, oblique turbulent flames is negligible. This assumption may require re-evaluation.

Velocity statistics conditional on ψ

As noted in the introduction, velocity statistics conditional on ψ, or distance from the flamelet, are useful for examining the changes in velocity which occur just across the flamelet, and for investigating the interaction between the flamelet and the flow– through examination of the variation in velocity statistics with proximity to the flamelet. In this section we see that the variation with flamelet position in both mean and rms velocities is sufficiently pronounced that the differences in conditional zone statistics may not accurately reflect the differences which occur just across the flamelet surface. In addition, examination of the variation in rms velocities provides information on the relative importance of turbulence generation by the flamelet

versus more conventional sources, such as enhanced generation by shear in the product gases.

Conditional statistics reported here are presented as a family of curves, each curve representing data obtained at a single spatial location of the LDV probe volume. Because only data obtained within the flame brush are presented, each spatial location is uniquely identified by the local reaction progress variable, $\langle c \rangle$, which serves to identify the curve. The conditional mean velocities presented below are shown for all values of ψ, as the variation of these quantities with ψ is smooth across the flamelet. Second order conditional statistics show a jump within the finite thermal flamelet thickness, due to the large variation in density (and consequently flow acceleration) within this region. Such jumps can be easily inferred from the conditional pdfs presented in Figs. 4 and 5. For greater clarity, the graphical presentation of these statistics excludes the flame regions, $\psi = -1$, 0, and 1. Excluding the results from these regions allows the true jump in the second order statistics across the flamelet to be seen more clearly. In addition, graphical clutter is reduced by presenting conditional statistics only at selected, representative lateral coordinates ($\langle c \rangle$). A full, tabulated set of the conditional statistics is available elsewhere[6].

Reference is made below to data obtained under other experimental conditions when such reference clearly amplifies or collaborates trends observed in the data presented here. For reasons of brevity these additional data are not presented, but are also available elsewhere in tabulated form[6].

Conditional profiles of mean lateral velocity are presented in Fig. 11. These profiles clearly demonstrate the variation of lateral velocity at a fixed point with proximity to the flamelet. Note that the variation in conditional mean lateral velocity within the reactants ($\psi > 1$) is most pronounced on the reactant side of the flame brush ($\langle c \rangle \approx 0.05$), where mean lateral velocities close to the flamelet can exceed the velocities further from the flamelet by as much as 30%. Similar behavior in conditional mean velocities within the products, on the product side of the flame brush, is observed only at an axial location of 30.0 mm. Under other flame conditions, this type of variation in the conditional mean may be seen throughout much of the flame brush, not only on the extreme reactant and product sides of the flame brush. We believe that errors and uncertainties in the experimental technique are of insufficient magnitude to be the cause of this behavior, and that it represents true evidence of interaction of the approach flow with the flame. As a result of this variation in the conditional mean velocity, the jump velocity across the flamelet may be larger than one

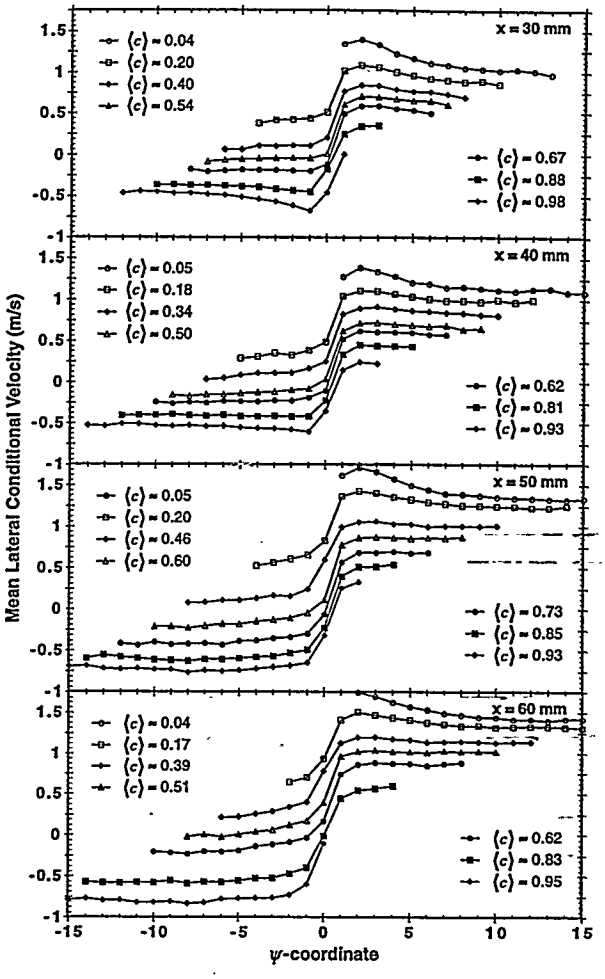

Figure 11: Profiles of the mean lateral velocity conditional on ψ. Positive ψ corresponds to data obtained within the unburnt reactants, while negative ψ corresponds to data obtained within the products. The ψ-coordinate can be interpreted as a measure of distance from the flamelet; an integral change in ψ corresponds to approximately 0.5 mm.

would infer from the difference between conditional reactant and product zone mean lateral velocities, although this effect is not prominent in the data presented here. Note that, as pointed out earlier, most of the acceleration in the mean flow is seen to take place across the flame regions, $\psi = -1$, 0, and 1.

Mean axial velocities conditional on ψ are shown in Fig. 12. This figure shows, at locations on the extreme reactant side of the flame brush, a decrease in the conditional mean axial velocity within the reactants as the flamelet is approached. This decrease is similar to the observed increase in conditional mean lateral velocities within the reactants. Within the central region of the flame brush, and on to the product side, however, an increase in the conditional mean velocities within the reactants is observed as the flamelet is approached.

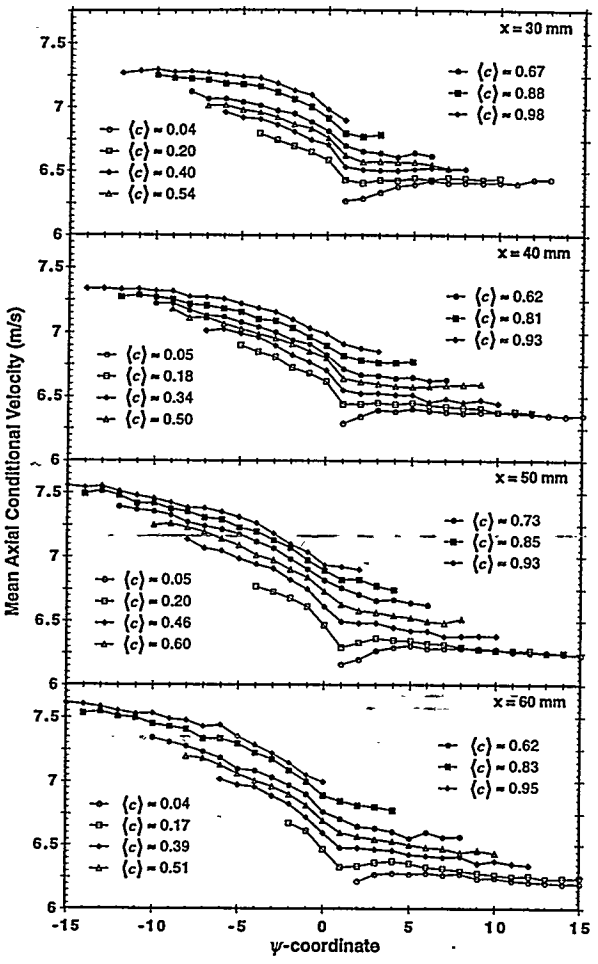

Figure 12: Profiles of the mean axial velocity conditional on ψ.

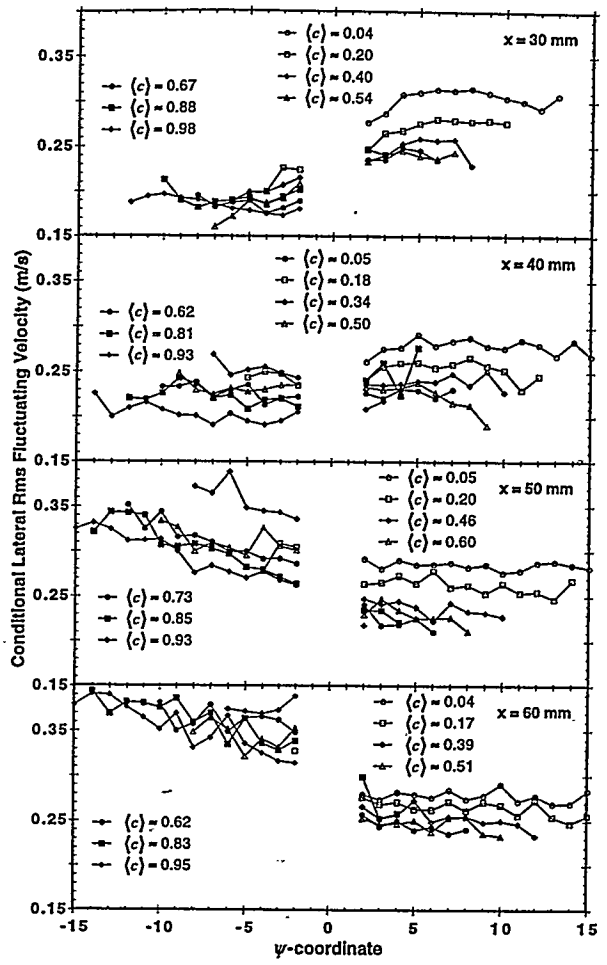

Figure 13: Profiles of the lateral rms fluctuating velocity conditional on ψ. Statistics computed for regions within the flamelet thermal thickness, $\psi = -1$, 0, and 1, are not shown.

Both behaviors clearly indicate a modification of the mean approach flow by proximity to the flamelet. Unlike the behavior seen in the conditional lateral mean velocities, the mean axial velocities indicate that the actual jump in the mean velocity across the flamelet is significantly smaller than what might be inferred from the difference in the conditional zone mean velocities, $\langle U_p \rangle - \langle U_r \rangle$. As noted earlier, the mean axial velocities conditional on ψ exhibit a relatively gradual variation with ψ. Indeed, the location of the flamelet may be difficult to discern in many of the profiles shown in Fig. 12.

Figure 13 shows the conditional lateral turbulence levels as a function of ψ. Here a clear variation with axial location is seen. At x=30.0 mm, the lateral turbulence levels are seen to decrease from reactants to products, while remaining approximately constant at x=40.0 mm. At x=50.0 mm and x=60.0 mm, the turbulence levels increase across the flamelet. The behavior of these conditional lateral turbulence levels is fully consistent with the conditional zone turbulence profiles presented above.

Two interesting aspects of these conditional statistics merit further discussion:

First, it is noted that at the lower axial locations the conditional turbulence levels within the reactants decrease as the flamelet is approached. This interesting behavior is observed (and may be much more pronounced) under other flame conditions as well. Under some conditions, turbulence levels within the reactants near the flamelet surface can be as low as 50% of the free-stream turbulence levels. Only at the higher axial locations do the turbulence levels within the reactants remain approximately constant, or perhaps increase slightly, with decreasing ψ. This observed reduction in reactant turbulence levels near the flamelet is of great interest. While conditional zone statistics at the lower axial locations may show a sharp drop in turbulence levels from reactants to products, the

statistics conditional on ψ show clearly that the actual drop in turbulence levels across the flamelet may be quite small.

Secondly, at the higher axial locations, the lateral turbulence levels within the products are seen to increase as ψ becomes more negative. That is, turbulence levels at a fixed point in space are higher when the flamelet is farther away. Under some flame conditions, this increase can be much more dramatic than that seen in Fig. 13. The observed increase in lateral turbulence levels with decreasing ψ is unlikely to be caused by measurement errors or shortcomings of the experimental technique (such as the effects of extreme flamelet orientations), which would only serve to mask this behavior. It is clear, therefore, that a significant proportion of the lateral component turbulence within the product gases is not associated with turbulence production by the flamelet but with other mechanisms of turbulence production.

Conditional statistics of axial turbulence levels are presented in Fig. 14, where a similar behavior to that seen in the conditional lateral component statistics is observed. At an axial location of 30.0 mm, axial component turbulence levels tend to remain approximately constant, or perhaps decrease slightly, from reactant to product fluid. As the axial location increases, axial component turbulence levels are seen to increase from reactants to products. Within the reactants (positive ψ), conditional turbulence levels decrease markedly as the flamelet is approached. In contrast to the lateral component results, the axial component turbulence levels within the products are seen to decrease as ψ becomes more negative. This decrease in conditional product gas turbulence levels as distance from the flamelet increases is remarkable, in that, as opposed to the lateral component turbulence, it indicates that a significant proportion of the axial component product zone turbulence is generated by the flamelet and not by other mechanisms of turbulence production.

It is also interesting to note that the increase in axial component turbulence levels across the flamelet is larger on the product side of the flame brush than on the reactant side. This conclusion may also be drawn from the conditional zone axial turbulence level profiles presented in Fig. 9. It is unlikely that shortcomings in the experimental technique could cause this behavior, and these results are believed to reflect a true flamelet/flow interaction phenomenon.

Comparing the jump in the lateral $(\Delta v' = \langle v_2'^2 \rangle^{1/2} - \langle v_1'^2 \rangle^{1/2})$ and axial $(\Delta u' = \langle u_2'^2 \rangle^{1/2} - \langle u_1'^2 \rangle^{1/2})$ component turbulence levels across the flamelet, it is seen that $\Delta u'$ exceeds $\Delta v'$ at all locations within the flame brush but on the extreme reactant side. This

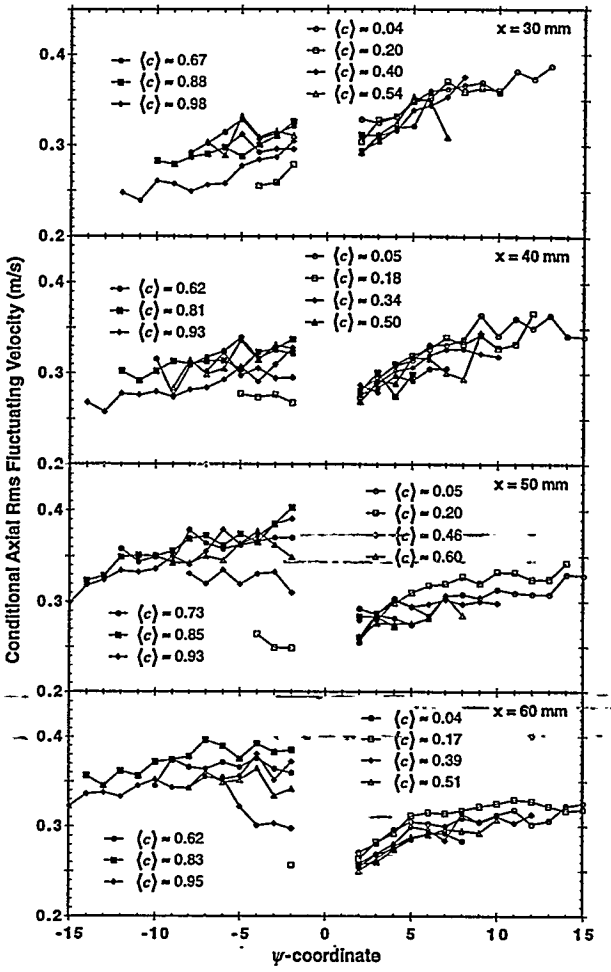

Figure 14: Profiles of the axial rms fluctuating velocity conditional on ψ.

observation, coupled with the above observation that a significant proportion of the lateral component turbulence appears to be generated by other mechanisms not associated with the flamelet, indicates that the turbulence which is produced by the flamelet is anisotropic, with the largest increase seen in the axial component. Although $\Delta u'$ and $\Delta v'$ may be negative in these flames (a decrease in turbulence levels across the flamelet), $\Delta u'$ is always observed to be greater than or approximately equal to $\Delta v'$. This anisotropic turbulence production by the flamelet is an important experimental observation. The axial component of velocity is more nearly tangential to the mean flamelet surface than the lateral component. As noted in the introduction, anisotropic turbulence production across the flamelet, with the tangential turbulence levels preferably enhanced, has been predicted theoretically[5]. To the knowledge of the authors, this prediction has not been previously confirmed.

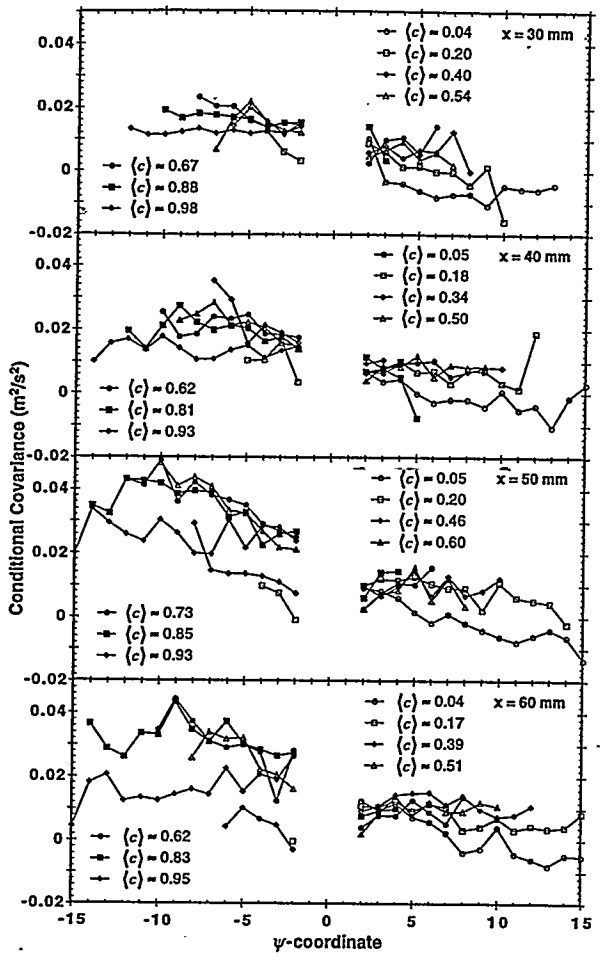

Figure 15: Profiles of the axial rms fluctuating velocity conditional on ψ.

Conditional velocity field covariances are presented in Fig. 15. The conditional covariance within the reactants is seen to remain approximately constant, perhaps increasing slightly, as the flamelet is approached. The covariance increases from reactants to products across the flamelet, except at points on the extreme reactant side of the flame brush. As noted in the discussion of the conditional zone statistics, the effects of extreme flamelet orientations will tend to make the measured covariance within the products negative, and these effects will be most pronounced at small values of ψ– near the flamelet surface. The observed increase in covariance across the flamelet is therefore expected to be an underestimate of the actual increase.

This increase and the positive sign of the conditional covariance are interesting not only as an indicator of the possible importance of generation of turbulence by shear within the products, but also as a further indicator of the anisotropic production of turbulence by the flamelet. If a transformation of coordinates were to be performed, into a coordinate system normal (η) and tangential (λ) to the mean flamelet surface, the following relationships would hold between the velocity field variances in the new coordinate system and the laboratory coordinate system:

$$\langle u_\eta'^2 \rangle = \langle u'^2 \rangle \sin^2\theta - 2\langle u'v' \rangle \sin\theta\cos\theta + \langle v'^2 \rangle \cos^2\theta \quad (6)$$

and

$$\langle u_\lambda'^2 \rangle = \langle u'^2 \rangle \cos^2\theta + 2\langle u'v' \rangle \sin\theta\cos\theta + \langle v'^2 \rangle \sin^2\theta, \quad (7)$$

where θ is the angle between the mean flamelet surface and the burner centerline. If the mean flamelet surface is defined to be oriented locally parallel to surfaces of constant $\langle c \rangle$, then $\theta \approx 18.5°$. From Eqs. (6) and (7) it is evident that, due to the positive covariance, anisotropic production of turbulence by the flamelet would be even more apparent in the new coordinate system.

Summary and Conclusions

An experimental technique which enables the simultaneous measurement of flamelet position and fluid velocity in premixed turbulent flames has been described. The interpretation of the data and the uncertainties involved have been discussed in detail to establish the validity of the data obtained.

The data are employed to compute conditional statistics of the velocity field, conditional both on zone (reactants or products) and on instantaneous distance from the flamelet. These statistics are presented and discussed with respect to their implications for modeling of premixed combustion, both statistical and analytical. The conditional statistics further permit the jumps in turbulence levels which occur just across the flamelet to be determined, and allow the interaction and modification of the turbulent velocity field by the flamelet to be examined.

Specifically, the following conclusions are made based on zone conditional statistics:

(1) The difference between the conditional zone mean velocities within the flame brush is observed to vary with both the axial and lateral coordinate in the oblique flame studied here. Models which express higher order velocity field statistics in terms of this difference must account for this variation.

(2) Reactant zone turbulence levels are observed to be higher than product zone turbulence levels at some spatial locations, lower at others. This variation implies that turbulence enhancement by flames is affected by local flow conditions.

(3) Product zone axial turbulence levels are found to vary considerably within the flame brush, indicating that flame generation of axial (near tangential to the

mean flame surface) velocity fluctuations is not constant within the flame brush.

(4) The sign and magnitude of the product zone covariance is such that mean flow shear is likely to be an important source of turbulence generation.

Additionally, statistics conditional on distance from the flamelet indicate:

(5) The jump in mean velocity which occurs just across the flamelet may not be well approximated by the difference in the zone mean velocities, due to variation in the mean flow associated with proximity to the flamelet. This mean flow variation is evidence of a strong flamelet/flow interaction.

(6) Fluctuating turbulent velocities within the reactants are observed to decrease with increasing proximity to the flamelet, further evidence of strong flamelet/flow interaction.

(7) Like the conditional zone statistics, turbulence levels are observed to increase across the flamelet at some locations and decrease at others.

(8) Product-gas, lateral-component fluctuating velocities are observed to decrease with increasing proximity to the flamelet, indicating that a significant amount of the turbulence is generated by mechanisms which are not associated with the flamelet.

(9) Product-gas, axial-component fluctuating velocities are observed to increase with increasing proximity to the flamelet, indicating that a significant amount of the axial turbulence is flamelet generated.

(10) Jumps in turbulence levels observed just across the flamelet are anisotropic– the largest increase (smallest decrease) is observed in the axial component.

(11) A jump in covariance to positive levels within the product gases is observed across the flamelet. This jump implies increased turbulence generation by shear in the product gases. Coupled with the observed anisotropy in the jumps in axial and lateral component turbulence levels, the positive covariance implies that fluctuating velocities tangential to the mean flamelet surface are preferentially enhanced over the fluctuating velocities normal to the mean flamelet surface.

Acknowledgments

The authors gratefully acknowledge the support of the U.S. Army Research Office, contract # DAAG29-82-K-0187 and the U.S. Department of Energy, Office of Basic Energy Sciences and Defense Programs Technology Transfer Initiative.

References

(1) Libby, P.A., "Theory of Normal Premixed Turbulent Flames Revisited," *Prog. Energy Combust. Sci.*, Vol. 11, 1985, pp. 83-96.

(2) Bray, K.N.C., Libby, P.A. and Moss, J.B., "Unified Modeling Approach for Premixed Turbulent Combustion- Part I: General Formulation," *Combustion and Flame*, Vol. 61, 1985, pp.87-102.

(3) Chen, J.-Y., Lumley, J.L., and Gouldin, F.C., "Modelling of Wrinkled Laminar Flames with Intermittency and Conditional Statistics," *Twenty-First Symposium (International) on Combustion*, The Combustion Institute, Pittsburgh, 1986, pp. 1483-1491.

(4) Clavin, P., "Dynamic Behavior of Premixed Flame Fronts in Laminar and Turbulent Flows", *Prog. Energy Combust. Sci*, Vol. 11, 1985, pp. 1-59.

(5) Clavin, P. and Williams, F.A., "Effects of Molecular Diffusion and of Thermal Expansion on the Structure and Dynamics of Premixed Flames in Turbulent Flows of Large Scale and Low Intensity," *J. Fluid Mechanics*, Vol. 116, 1982, pp. 251-282.

(6) Miles, P.C., "Conditional Velocity Statistics and Time-Resolved Flamelet Statistics in Premixed Turbulent V-Shaped Flames," Ph.D. Thesis, Cornell University, Ithaca, NY, 1991.

(7) Cheng, R.K., "Conditional Sampling of Turbulence Intensities and Reynolds Stress in Premixed Turbulent Flames," *Combustion Science and Technology*, Vol. 41, 1984, pp.109-141.

(8) Cheng, R.K., Talbot, L., and Robben, F., "Conditional Velocity Statistics in Premixed CH_4-Air and C_2H_4-Air Turbulent Flames," *Twentieth Symposium (International) on Combustion*, The Combustion Institute, Pittsburgh, 1984, pp. 453-461.

(9) Westbrook, C.K., Dryer, F.L., and Schug, K.P., "Numerical Modeling of Ethylene Oxidation in Laminar Flames," *Combustion and Flame*, Vol. 52, 1983, pp. 299-313.

(10) Abraham, J., Williams, F.A, and Bracco, F.V., "A Discussion of Turbulent Flame Structure in Premixed Charges," SAE Paper 850345, Society of Automotive Engineers, Detroit, 1985.

(11) Cattolica, R.J., Barr, P.K., and Mansour, N.N., "Propagation of a Premixed Flame in a Divided-Chamber Combustor," *Combustion and Flame*, Vol. 77, 1989, pp. 101-121.

(12) Miles, P. and Gouldin, F.C., "Fully-conditional Velocity Measurements in Premixed Turbulent Flames," *Chemical and Physical Processes in Combustion*, Fall Technical Meeting, Eastern Section of the Combustion Institute, 1988, pp.4.1-4.4.

(13) Stairmand, C.J., "The Design and Performance of Cyclone Separators," *Trans. Inst. Chem. Eng.*, Vol. 29, 1951, pp. 356-383.

(14) Dirgo, J. and Leith, D., "Cyclone Collection Efficiency: Comparison of Experimental Results with Theoretical Predictions," *Aerosol Science and Technology*, Vol. 4, 1985, pp. 401-415.

(15) Ikioka, L.M., Brum, R.D., and Samuelson, G.S., "A Laser Anemometer Seeding Technique for Combustion Flows with Multiple Stream Injection," *Combustion and Flame*, Vol. 49, 1983, pp.155-162.
(16) Raabe, O.G., "The Generation of Aerosols of Fine Particles," *Fine Particles*, edited by B.Y.H. Liu, Academic Press, 1976, pp. 57-110.
(17) Chew, T.C., Britter, R.E., and Bray, K.N.C., "Laser Tomography of Turbulent Premixed Bunsen Flames," *Combustion and Flame*, Vol. 75, 1989, pp. 165-174.
(18) Miles, P. and Gouldin, F.C., "Simultaneous Measurements of Flamelet Position and Gas Velocity in Premixed Turbulent Flames," *Proceedings of ASME-JSME Thermal Engineering Joint Conference*, Vol. 1, Honolulu, Hawaii, 1987, pp. 187-193.
(19) Holman, J.P., *Experimental Methods for Engineers*, McGraw-Hill, 1978.
(20) Miles. P.C. and Gouldin, F.C., "Mean Reaction Rates and Flamelet Statistics for Reaction Rate Modelling in Premixed Turbulent Flames," *Twenty-Fourth Symposium (International) on Combustion*, The Combustion Institute, Pittsburgh, 1992, pp.477-484.